

**PCCP****Polyamidoxime Chain Length Drives Emergent Metal-Binding Phenomena**

Journal:	<i>Physical Chemistry Chemical Physics</i>
Manuscript ID	CP-ART-04-2018-002198.R1
Article Type:	Paper
Date Submitted by the Author:	17-Sep-2018
Complete List of Authors:	Earl, Lyndsey; Oak Ridge National Laboratory Do, Changwoo; Korea Advanced Institute of Science and Technology, Department of Nuclear and Quantum Engineering; Oak Ridge National Laboratory, Biology and Soft Matter Division Wang, Yangyang; Oak Ridge National Laboratory, Center for Nanophase Materials Sciences Abney, Carter; Univ of Chicago, Dept of Chem

SCHOLARONE™
Manuscripts



Journal Name

ARTICLE

Notice of Copyright:

This manuscript has been co-authored by UT-Battelle, LLC, under contract DE-AC05-00OR22725 with the US Department of Energy (DOE). The US government retains and the publisher, by accepting the article for publication, acknowledges that the US government retains a nonexclusive, paid-up, irrevocable, worldwide license to publish or reproduce the published form of this manuscript, or allow others to do so, for US government purposes. DOE will provide public access to these results of federally sponsored research in accordance with the DOE Public Access Plan (<http://energy.gov/downloads/doe-public-access-plan>).

Received 00th January 20xx,
Accepted 00th January 20xx

DOI: 10.1039/x0xx00000x

www.rsc.org/

Polyamidoxime Chain Length Drives Emergent Metal-Binding Phenomena

L. D. Earl,^{a†} C. Do,^{b*} Y. Wang,^c and C. W. Abney^{a§*}

Emergence is complex behavior arising from the interactions of many simple constituents that do not display such behavior independently. Polyamidoxime (PAO) uranium adsorbents show such phenomena, as recent works articulate the polymer binds uranium differently than the monomeric constituents. In order to investigate the origins of this emergent uranium-binding behavior, we synthesized a series of amidoxime polymers with low polydispersity and small molecules with lengths ranging from 1 to 125 repeat units. Following immersion in a uranyl-containing solution, the local, intermediate, and macroscopic structures were investigated by x-ray absorption fine structure (XAFS) spectroscopy, small angle neutron scattering (SANS), and dynamic light scattering (DLS). Fits of the extended XAFS (EXAFS) region revealed a progressive change in uranium coordination environment as a function of polymer molecular weight, identifying chain length as a driving force in emergent metal binding and resolving the controversy over how amidoxime adsorbents bind uranium.

Introduction

Emergent phenomena is loosely defined as the complex outcome arising from the correlated interactions of many simple constituents that individually do not display such behaviour. Nature is replete with instances of emergence, with diverse examples ranging from the atomic – e.g. fractals formed by water freezing or neurons in the brain forming human consciousness – to the macroscopic – such as the murmuration of starlings or formation of ripple patterns in sand dunes. At the molecular scale, uncovering the fundamental rules of correlations and emergence is essential to enable their manipulation and the subsequent preparation of new materials and processes.¹ While previously reported designer systems²⁻⁴ afford elegant examples of the inherent potential, it is another matter to take a complex material displaying emergent behaviour and deconvolute the physicochemical processes to afford understanding and enable control.

One such system is the current state-of-the-art material developed for recovery of seawater uranium: a polymeric adsorbent composed of poly(amidoxime) graft chains covalently bound to a polyolefin trunk.⁵⁻⁸ Over the past 35 years,⁹⁻¹³ the performance of these materials has improved nearly tenfold based on the optimization of synthetic parameters¹⁴⁻¹⁶ and adaptation of advanced polymerization techniques,¹⁷ yet true technological breakthrough is stymied by a lack of fundamental knowledge regarding the structure-function relationship of soft materials. Although descriptions of adsorbent-metal interactions exist by way of computational

studies¹⁸⁻²¹ and investigation of crystal structures from small molecule analogs,²²⁻²⁵ recent research has demonstrated this established paradigm does not correctly describe the uranyl binding environment following capture by amidoxime-functionalized polymer adsorbents from environmental seawater.^{26, 27} While this discrepancy in binding mode was attributed to the occurrence of emergent phenomena, the physical origins of this behaviour nevertheless remain entirely unknown.

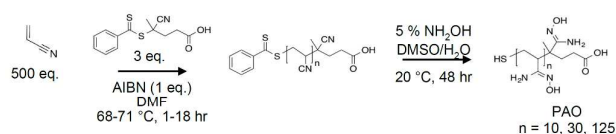


Figure 1. Overview of polyamidoxime synthesis.

Previous research has demonstrated that both trunk surface area^{28, 29} and graft composition^{5, 15, 16, 30-32} strongly influence the performance of the resulting adsorbent though increased mass transport,³³ greater binding site density, and by influencing the graft chain morphology.¹⁷ Metal-polymer interactions, such as ion-crosslinking with divalent cations ubiquitous in seawater, are also known to cause changes in the mesoscale structure of tethered graft polymers.³⁴⁻³⁶ Furthermore, strong hydrogen-bonding has been documented in amidoximes and amidoxime-derived systems,³⁷ with disruption of these interactions a potential explanation for the adsorbent base-conditioning required prior to deployment in seawater. Although the aforementioned physical interactions are known, a satisfactory model to describe the intra- and interpolymer interactions and metal-adsorbent interfacial interactions does not exist for these complex, heterogeneous systems, and no information is available pertaining to the interplay between polymer structure and metal coordination environment. Moreover, at a fundamental level, little work has been done in an effort to investigate the manner in which molecular interactions compound to induce intermediate and mesoscale morphological behaviour in polymer adsorbents.

^a Chemical Sciences Division, Physical Sciences Directorate, Oak Ridge National Laboratory, One Bethel Valley Road, P.O. Box 2008, Oak Ridge, TN 37831, USA

^b Neutron Scattering Division, Oak Ridge National Laboratory, One Bethel Valley Road, P.O. Box 2008, Oak Ridge, TN 37831, USA

^c Center for Nanophase Material Sciences, Physical Sciences Directorate, Oak Ridge National Laboratory, One Bethel Valley Road, P.O. Box 2008, Oak Ridge, TN 37831, USA

† Electronic Supplementary Information (ESI) available: A document containing general synthetic, characterization, and experimental details; XAFS data collection and processing details; SANS data collection and processing details; supplementary data and figures (pdf). See DOI: 10.1039/x0xx00000x

In this work we provide the first report of the influence of polymer length on the coordination environment of a bound metal, and characterize the influence of such molecular-scale interactions on the resulting intermediate and mesoscale structure. To these ends, a series of unsupported amidoxime polymers were synthesized as a model system, allowing fine control over chain length and facilitating direct investigation of the resulting chain morphology. The polyamidoximes were subsequently contacted with a sub-stoichiometric amount of $\text{UO}_2(\text{NO}_3)_2$ and interrogated through application of X-ray absorption fine structure (XAFS) spectroscopy, small angle neutron scattering (SANS), and dynamic light scattering (DLS). Notably, these techniques afford structural information spanning molecular, intermediate, and mesoscale spatial regimes, proving critical for identifying the origins of emergent binding phenomena and enabling the rational design and development of advanced forms of soft material.

Experimental

Polymer Synthesis

Polyacrylonitrile (PAN) precursors were synthesized using a RAFT polymerization procedure, with chain length controlled by variation of reaction time;^{38, 39} the accompanying polyamidoximes were obtained through conversion of the nitrile group by treatment with hydroxylamine (Figure 1).^{40, 41} It is well established that polymer length directly affects bulk physical properties which necessarily arise from small compounding differences occurring in the convolution of their individual molecular constituents. Accordingly, a series of unsupported low molecular weight polymers were synthesized, spanning a representative range of the proposed lengths for the graft chain on polyamidoxime adsorbents. Details regarding the experimental procedure and material characterization are provided in the Supporting Information. The conversion of PAN to PAO was confirmed using IR spectroscopy (Figures S1-S2), specifically by monitoring the disappearance of the nitrile peak at 2245 cm^{-1} with commensurate appearance of the oxime C=N stretch at 1640 cm^{-1} and a hydrogen bonded species at $3000\text{--}3500\text{ cm}^{-1}$. End group analysis of ^1H NMR spectra was used as a method of determining polymer chain length of the PAN precursors (Figures S3-S8), while gel permeation chromatography – size exclusion chromatography (Figure S9-S10) verified the relative molecular weights and confirmed suitable polydispersity of the higher molecular weight PAN precursors (1.15 – 1.21) and polyamidoximes (1.20 – 1.28) (Table S3).

X-ray Absorption Spectroscopy

To investigate the effect of polymer chain length on metal binding environment, XAFS spectra were collected at beamline 11-2 of the Stanford Synchrotron Radiation Lightsource at the uranium L_{III} -edge (17166 eV) for solutions of $5\text{ mM UO}_2(\text{NO}_3)_2$ in DMSO containing approximately 3 mg/mL polyamidoxime, affording 25 mM total amidoxime binding sites. Two control samples were also analysed, consisting of the acrylamidoxime

small molecule with $\text{UO}_2(\text{NO}_3)_2$ in DMSO, and $\text{UO}_2(\text{NO}_3)_2$ dissolved in DMSO without any amidoxime species. While evaluating the fits of the polymer solutions, discussed below, we assumed uranyl-amidoxime interactions dominate over uranyl-nitrate or uranyl-solvent interactions. This assumption is supported by a difference in the colour of solutions containing polyamidoxime (light brown) versus that of the control (dark yellow), as well as recent computational and small molecule investigations which demonstrate strong interactions of uranyl with amidoxime.^{22, 24, 42-44} Data were processed and fit using the Athena and Artemis programs of the IFEFFIT package based on Feff 6.^{45, 46} Additional details on data collection, processing, and fitting are provided in the ESI.

Small Angle Neutron Scattering

The morphology of the polymer systems before and after uranyl binding was interrogated through SANS, collected on Beamline-6, EQ-SANS, at the Spallation Neutron Source of Oak Ridge National Laboratory.⁴⁷ Samples were prepared under identical metal to polymer ratios as in XAFS experiments, but at a three-fold higher concentration in DMSO- d_6 to improve counting statistics. Data were reduced and processed using MantidPlot using standard procedures to correct for detector sensitivity, instrument dark current, sample transmission, and empty cell background.⁴⁸

Dynamic Light Scattering

Dynamic light scattering experiments were conducted at $25\text{ }^\circ\text{C}$ using an ALV compact goniometer system with 7002 Multiple Tau Digital Correlator. The wavelength of the incident light from the Helium-Neon laser was 632.8 nm . Disposable borosilicate glass culture tubes were used as sample cells and were cleaned prior to use within a reflux apparatus to remove dust. Samples were prepared at a concentration of 3 mg mL^{-1} polymer in $4.5\text{ mM UO}_2(\text{NO}_3)_2 \cdot 6\text{ H}_2\text{O}$ in DMSO and filtered through a $0.45\text{ }\mu\text{m}$ PTFE filter. Additional details on data analysis are provided in the ESI.

Results and Discussion

Although acetamidoxime possesses significant polarity, in our hands, polyamidoxime displayed little solubility in water, even following addition of urea denaturant to mitigate potential hydrophobic effects.⁴⁹ Early works articulate significant improvement in uranium uptake upon inclusion of hydrophilic comonomers, with grafting solutions typically containing between $30\text{ -- }40\%$ for optimal performance.³⁰⁻³² However, recently developed adsorbents contain comparatively little comonomer in the final material,^{15, 16} and adsorbents prepared by conversion of pure PAN grafts are still actively investigated.^{50, 51} This simple observation thus has important implications for the development of adsorbents for seawater uranium recovery. Neutral polymer brushes form pinned micelles when tethered to a surface at low grafting densities and immersed in a poor solvent.⁵² Such micelles form to minimize exposed surface area, with the resulting

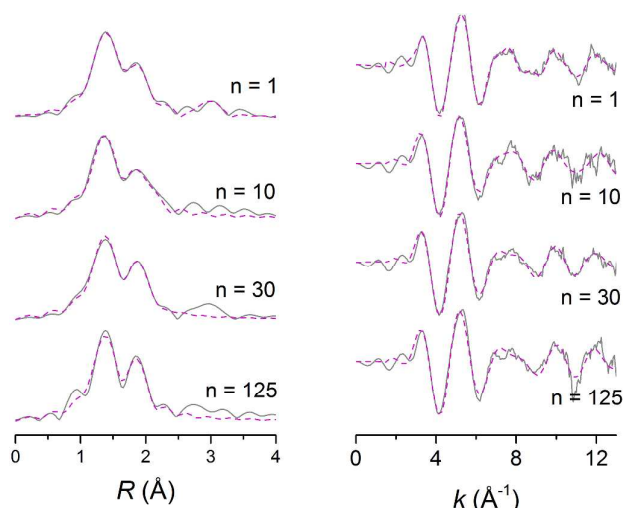


Figure 2 Uranium L_{III} -edge EXAFS spectra for sub-stoichiometric UO_2^{2+} solutions of $UO_2(NO_3)_2$ and molecules with $n_2 = 1$, $n = 10$, $n = 30$, and $n = 125$ amidoxime repeat units, displayed with a k -weighting. Fits are plotted as (left) the magnitude of the Fourier transform in real space and (right) in k -space. Data were fit from 1 – 2.5 in R -space and 3 – 12.6 in k -space.

morphology having a clearly deleterious effect on adsorbent performance. Due to the improved solubility of the polymer in polar aprotic solvents, we used DMSO for UO_2^{2+} -polymer XAFS, SANS, and DLS investigations. Additionally, this solvent choice allowed observation of UO_2^{2+} -polymer interactions in the absence of protic media, eliminating the influence of hydrogen bonding with solvent and the commensurate effects on polymer morphology.

The extended XAFS (EXAFS) spectra for the aforementioned samples and their accompanying fits are displayed in Figure 2. The dominant feature at $R \approx 1.4 \text{ \AA}$ ⁵⁶ is assigned to the tightly bound axial oxygens of the uranyl cation while the second major feature ($R \approx 1.9 \text{ \AA}$) corresponds to scattering from equatorially-bound light (e.g. N, O) atoms. Features occurring beyond this are attributed to single scattering paths of atoms not directly bound to uranium, as well as multiple scattering paths. Investigation of crystal structures reveal $U-O_{eq}$ bond lengths for monodentate-bound amidoxime are approximately 0.1 \AA shorter than η^2 -bound amidoxime.^{22, 23, 43} Therefore, fits of the EXAFS data for uranyl-contacted polymer samples were performed using a structure model composed a variable number of equatorial oxygen located at 2.30 \AA and 2.44 \AA from the uranium atom (denoted “short” and “long,” respectively), in addition to the two tightly-bound axial oxygen of uranyl (Figure 3). As the degeneracy of scattering paths is directly correlated with the amplitude

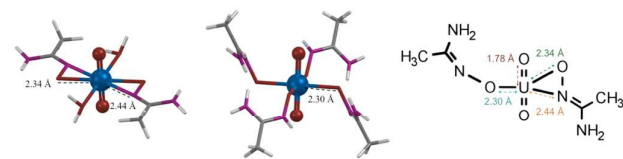


Figure 3 Structure models of oxygens used to fit the EXAFS data for uranyl-contacted polymer samples.

reduction factor (S_0^2), a value for S_0^2 was obtained by fitting the control spectrum of $UO_2(NO_3)_2$ (Figure S11, Tables S5-6) and defined in subsequent fits of the polymers and small molecule sample. Degeneracy and change in $U-O_{eq}$ distance for both equatorial oxygen scattering paths were allowed to vary, however restraints were imposed to ensure the number of equatorially coordinating atoms was physically reasonable, based on the maximum and minimum equatorially-coordinating atoms in the crystal structures.^{22, 23, 43} The results of the refined fits are displayed in Table 1, with additional details on the fitting model provided in the SI.

Analysis of the refined parameters for the nearest neighbour fit of the UO_2 -acetamidoxime small molecule sample reveals two atoms at 2.46 \AA , suggestive of a 2:1 complex of UO_2^{2+} and η^2 -bound amidoximate, and corroborated by comparison with the previously-published EXAFS data of the crystalline η^2 -bound $UO_2(\text{benzamidoxime})_2(\text{MeOH})_2$.²⁶ This first shell fit of the small molecule system is displayed in Figure S12. Of the remaining light scatterers in the equatorial plane at 2.31 \AA , two can be assigned to the amidoxime, while the remainder (1.5) are from coordinating DMSO. This assignment is confirmed by a subsequent fit over a longer range in R -space that fixes the first shell path lengths and includes a $U-S_{DMSO}$ scattering path at 3.58 \AA , distant scattering paths from bound amidoxime, and multiple scattering contributions from the axial $U=O$ (Figure S13, Table S7).

Table 1. Refined fit of uranyl-contacted polymers and controls in DMSO

Length	$U-O_{short} (\text{\AA})$	$\sigma^2 (\times 10^{-3} \text{\AA}^2)$	$U-O_{long} (\text{\AA})$	$\sigma^2 (\times 10^{-3} \text{\AA}^2)$
$n = 1$	2.31 ± 0.003	4 ± 1	2.46 ± 0.08	4 ± 1
$n = 10$	2.31 ± 0.03	2 ± 1	2.47 ± 0.03	2 ± 1
$n = 30$	2.34 ± 0.04	2 ± 1	2.45 ± 0.03	2 ± 1
$n = 125$	2.36 ± 0.03	2.9 ± 0.8	2.5 ± 0.1	2.9 ± 0.8

In contrast, polymer samples were all well fit using only two single scattering paths for the equatorial atoms. While a fit over a larger range in R -space was attempted, similar to the small molecule sample, improvements in the fits through inclusion of more distant scattering paths (e.g. the $U-S_{DMSO}$ path at 3.58 \AA) were not statistically significant based on application of the Hamilton Test.⁵³⁻⁵⁵ This lead us to conclude coordination by DMSO was negligible for the polymeric samples and the minor features likely due to the convolution of scattering paths afforded by the polymer in the second coordination sphere. Though these outer sphere contributions cannot be deconvoluted and refined to afford meaningful atomic information, including this region of R -space in the analysis would increase the number of independent points in our data, potentially allowing us to over-parameterize the fit. Thus, to obtain the most robust and physically defensible results possible, we reduced our fitting window in R -space to only include scattering paths from the atoms directly bound to UO_2^{2+} .

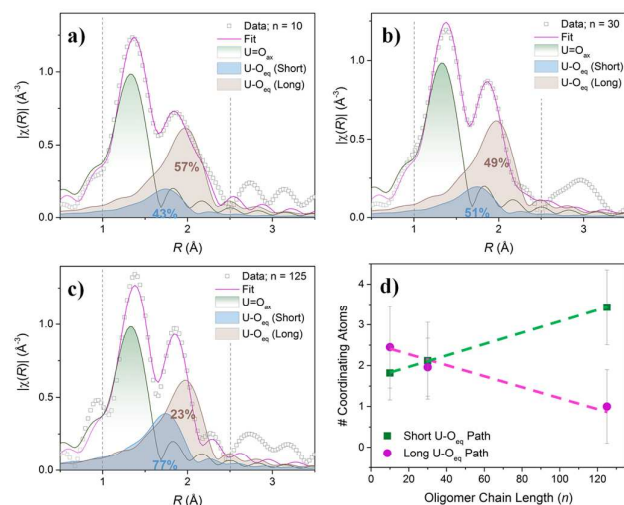


Figure 4. (a-c) Contributions of select scattering paths used to fit uranium L_{III} -edge EXAFS spectra data collected on polymer systems. Data are displayed as open grey squares, the fit is a solid magenta line, the $U=O_{ax}$ scattering path is in green, and $U-O_{eq}$ scattering paths for 2.30 \AA ("short") and 2.44 \AA ("long") are displayed in blue and brown, respectively. For the equatorial scattering paths, the percent contribution to the total number of equatorial scatterers is displayed within the path. Panels display fits for (a) $n = 10$, (b) $n = 30$, and (c) $n = 125$ amidoxime repeat units. (d) Number of equatorially coordinating atoms for short and long $U-O_{eq}$ scattering paths as a function of polymer length. The predominant contribution to the equatorial scattering changes as a function of polymer length supporting a change in binding mode. Dashed lines are guides for the eye.

Significant differences are observed in terms of how the uranyl coordination environment changes as a function of polymer chain length (Figure 4d). For the short chain ($n = 10$) polymer, the major contribution to the uranyl equatorial coordination environment is at a distance of 2.47 \AA , consistent with primarily η^2 -binding. While approximately equal contributions are observed for the intermediate system ($n = 30$), a short 2.36 \AA scattering path clearly predominates for the long polymer ($n = 125$), indicative of monodentate coordination. The inversion of contributions from the two scattering paths indicate the of different molecular weight, and supports the emergence of a different metal-binding mode as contingent upon polymer chain length.

Although unanticipated by traditional paradigms, the coordination mode for adjacent amidoximes in a polymer has never been definitively determined. Even after the η^2 binding mode was established for coordination of individual acetamidoxime molecules crystallographically,^{22, 43} computationally,^{22, 44} and by previous EXAFS studies,⁵⁶ Rao and colleagues nevertheless favoured bis-monodentate binding for the propyl-bridged glutardiamidoxime, based on an analysis of the stability constants associated with formation of UO_2^{2+} complexes.²⁴ Furthermore, EXAFS analysis of seawater-exposed polymer adsorbents also revealed UO_2^{2+} was clearly not bound in an η^2 mode by the amidoxime group on the graft chain.^{26, 27} From these previously reported results, one must rationalize there exists a point between small molecule and graft polymer at which the coordination mode for UO_2^{2+} is no longer η^2 , further substantiated by the findings reported above. Furthermore, while evaluating coordination

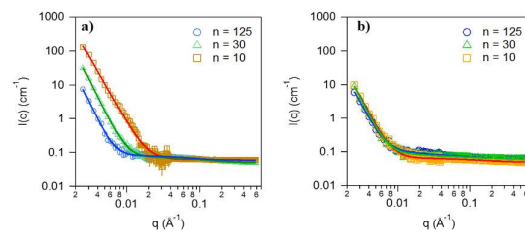


Figure 5: Small angle neutron scattering of a) polyamidoxime (10 mg mL^{-1}) in DMSO b) UO_2^{2+} contacted polyamidoxime in DMSO. Lines show the fit of the data.

environment is a common exercise when analysing XAFS data,^{57, 58} we found no reports of coordination environment being evaluated from the vantage point of the physical length of a polymer. XAFS has been used to support and quantify structural changes observed from SAXS experiments on pyridine-polyurethanes blended metal acetates,⁵⁹ but not to describe solution state metal structure as a function of polymer length. In addition to providing an important aspect for the consideration of adsorbents for the recovery of seawater uranium, this result also constitutes the first demonstration that a metal binding environment can be controlled through tuning of polymer chain length, providing essential foundational knowledge for the design and control of functional soft matter.

Having identified a correlation between metal coordination environment and polymer chain length, we sought to directly investigate the polymer morphology pre- and post-contact with $UO_2(NO_3)_2$ by SANS. Figure 5a shows the scattering intensity as a function of the scattering vector q for polymers with $n = 10, 30$, and 125 in the presence and absence of UO_2^{2+} . Inspection of the SANS data prior to contact with UO_2^{2+} reveals formation of aggregates for all polymer lengths, and the size of the aggregates are clearly correlated with chain length. Due to instrument limitations in q range and the reciprocal relationship between q and R_g , the radius of gyration, scattering intensity below 0.005\AA^{-1} cannot be ascribed to physical structure, though a coarse approximation indicates the aggregates are in excess of $\sim 65 \text{ nm}$ in dimension for all systems (Table 2). Porod analysis of the scattering data from 0.005 to 0.01 affords a log-log slope of $q^{-3.7}$ for the polymer with $n = 10$, indicative of a rough interface with surface fractal structuring. In contrast, a slope in excess of q^{-4} is observed for $n = 30$ and 125 , comprising a negative deviation from Porod's approximation, indicating the electron density across the surface is not well represented by a Heaviside (step) function.⁶⁰ This occurs when the interface of the aggregate structure is diffuse, and is known to occur for low-crystalline polymers where there is a gradual transition of the scattering length density, $\rho(r)$, at the boundary.⁶⁰

Table 2. Fit of slope of Porod region of SANS data

Length	UO ₂ ²⁺ -Contacted	Metal Free
n = 10	4.4 ± 0.1	3.70 ± 0.02
n = 30	4.2 ± 0.1	4.35 ± 0.03
n = 125	3.95 ± 0.01	4.1 ± 0.1

SANS data show that contact of the polymers with UO₂²⁺ resulted in overall very large aggregates of a size that is outside the length scale that the instrument can quantify. While marked differences are apparent for the metal-free polymer solutions, the data sets are effectively indistinguishable following exposure to UO₂²⁺. The upturns at low-q that are almost identical for all systems, as shown in Figure 5b, suggest formation of very large aggregates. While the limited q-range available from the SANS data prevents estimation of the size of the aggregates in the presence of UO₂²⁺ in DMSO, the shift of scattering curve of the shortest length polymers after the UO₂²⁺ contact was most significant of all polymers. (Supporting Information) Although less prominent, a similar transition is also observed with polymers with n = 30. One possible interpretation is that metal ions cross-link the polyamidoxime aggregate structures, similar to phenomena observed in liquid/liquid separations performed with amphiphilic extractants,⁶¹⁻⁶³ and suggesting these more thoroughly investigated systems may provide insight to metal binding behaviour of polymer adsorbents.

In order to better visualize the aggregation effects in these longer spatial regimes, dynamic light scattering (DLS) experiments were also performed on solutions of UO₂²⁺-polyamidoxime in DMSO. Decay times for the DLS experiments were obtained using the regularized inverse Laplace transform method, and the time decays were converted to hydrodynamic radii (R_h) using the Stokes-Einstein relation. R_h for polyamidoxime and UO₂²⁺-polyamidoxime are summarized in Table 3. Apart from the shortest polymer following contact with UO₂²⁺, two features are present within the size distribution plots for all samples, with the smaller feature ascribed to single polymer units while the larger feature is assigned to aggregate structures. Again with the exception of the shortest polymer, agglomerate size is not influenced by the presence of UO₂²⁺ and is only weakly associated with the polymer length. However, a slight contraction of R_h does occur for the single polymer when UO₂²⁺ is added to the system. This result confirms the presence of UO₂²⁺ influences the chain conformation of polyamidoxime, albeit to a modest extent. These results are consistent with those obtained by EXAFS, revealing the changes observed at the molecular extend to longer length scales, and thus demonstrating metal binding has an appreciable effect on graft chain morphology.

Table 3. R_h for solutions of polymers in the presence and absence of UO₂²⁺

Length		R _h (nm) (aggregate)	R _h (nm) (single polymer)
n = 10	Not Contacted	125	3.5
	UO ₂ ²⁺ Contacted	65	-
n = 30	Not Contacted	130	4.5
	UO ₂ ²⁺ Contacted	130	4
n = 125	Not Contacted	200	5.5
	UO ₂ ²⁺ Contacted	200	5

As revealed by SANS and DLS, the longest polymers displayed negligible change in intermediate structure following contact with UO₂²⁺, suggesting the solvent-polymer interactions impose greater energetic constraints than those induced following UO₂²⁺ cross-linking. Interpreting this data in light of the EXAFS results and previously reported computational studies,²² we conclude the constrained long-chain polymer structure cannot reorganize to accommodate a thermodynamically ideal η²-binding configuration. As a result, the bound UO₂²⁺ displays a different binding mode than is predicted from small molecule^{22, 43, 64} and computational investigations.^{21, 22, 65} Future work relying on findings obtained from such studies must therefore also consider the role of the polymer structure and influence of solvent on the uranium binding mode and energetics.

Conclusions

In conclusion, a series of unsupported polyamidoximes dissolved in DMSO were employed as an initial model for describing supported polyacrylamidoxime adsorbents for uranium recovery from seawater. From a practical perspective, it is critical to note the insolubility of these polymers in water under environmentally-relevant pH. This affords a highly plausible explanation why uranium uptake does not increase linearly with additional degree of grafting: hydrophobicity and significant self-affinity of drive irreversible graft chain collapse, preventing access to all but the very surface metal binding sites. EXAFS analysis of the UO₂²⁺-contacted polymer solutions reveals a change in uranyl binding mode as a function of polymer length, transitioning from η²-binding for the shortest polymer to a monodentate or chelating mode for longer polymers, with roughly equal contributions of the two modes observed for the polymer possessing approximately 30 repeat units. This provides the first evidence that at least one contribution to previously reported emergent metal binding phenomena can be ascribed to increasing graft chain length, and as a corollary, controlling polymer length affords an approach to rationally manipulate metal binding environments. SANS and DLS measurements revealed formation of aggregates for all polymers, with a noteworthy contraction observed upon exposure to UO₂²⁺. The shortest polymer displayed the greatest sensitivity to metal ion contact, suggesting a greater degree of freedom and flexibility to distort and afford optimal metal-receptor interactions, while the longest polymer displayed little change

upon exposure to UO_2^{2+} , suggesting a structurally restrained configuration. Interpreted consistently with the EXAFS data, this suggests chain entanglement or differences in solvation energetics may drive changes in binding environment and be a critical factor in the emergent phenomena observed in soft matter.

Acknowledgements

LDE and CWA were supported by the U.S. Department of Energy, Office of Nuclear Energy, under Contract DE-AC05-00OR22725 with Oak Ridge National Laboratory, managed by UT-Battelle, LLC. Research at Oak Ridge National Laboratory's Spallation Neutron Source and Oak Ridge National Laboratory's Center for Nanophase Materials Science was sponsored by the Scientific User Facilities Division, Office of Basic Energy Sciences, U.S. Department of Energy.

Use of the Stanford Synchrotron Radiation Lightsource, SLAC National Accelerator Laboratory, is supported by the U.S. Department of Energy, Office of Science, Office of Basic Energy Sciences under Contract No. DE-AC02-76SF00515. A portion of this research used resources at the Spallation Neutron Source, a U.S. Department of Energy (DOE) Office of Science User Facility operated by the Oak Ridge National Laboratory. This work benefitted from SasView software, originally developed by the DANSE project under NSF award DMR-0520547. This manuscript has been authored by UT-Battelle, LLC under Contract No. DE-AC05-00OR22725 with the U.S. Department of Energy. Polymer characterization was performed at Oak Ridge National Laboratory's Center for Nanophase Materials Science, which is a DOE Office of Science User Facility.

The United States Government retains and the publisher, by accepting the article for publication, acknowledges that the United States Government retains a non-exclusive, paid-up, irrevocable, worldwide license to publish or reproduce the published form of this manuscript, or allow others to do so, for United States Government purposes. The Department of Energy will provide public access to these results of federally sponsored research in accordance with the DOE Public Access Plan (<http://energy.gov/downloads/doe-public-access-plan>).

Notes and references

‡ LDE Current Address: Intel Corporation, 2501 NW Century Blvd, Hillsboro, OR 97124

§ CWA Current Address: ExxonMobil Research & Engineering, 1545 US-22 #1, Annandale, NJ 08801

§§ The EXAFS signal depends on $\sin[2kRi + \delta_i(k)]$, where k is the energy of the photoelectron in wavenumbers, R is the half-path length of the i th scatterer, and $\delta_i(k)$ is the phase shift of the photoelectron. In this work we generally refer to the crystallographic positions of the atoms in terms of their actual distance in Å from uranium. However, their contributions to the Fourier transform of the data are discussed in terms of their radial distance in Å, uncorrected for $\delta_i(k)$. As a result, plots of the Fourier transform display features attributable to

atoms which are farther away than is indicated by the x -axis. While 2 Å is clearly a distance at which bonding occurs, features occurring beyond 2 Å in the Fourier transformed EXAFS spectra generated by backscattering from light atoms possess half-path lengths (i.e. bond lengths) greater than 2.7 Å.

1. J. Hemminger, G. Fleming and M. Ratner, *Directing Matter and Energy: Five Challenges for Science and the Imagination*, U.S. Department of Energy, 2007.
2. M. I. H. Mohideen, B. Xiao, P. S. Wheatley, A. C. McKinlay, Y. Li, A. M. Z. Slawin, D. W. Aldous, N. F. Cessford, T. Düren, X. Zhao, R. Gill, K. M. Thomas, J. M. Griffin, S. E. Ashbrook and R. E. Morris, *Nat. Chem.*, 2011, **3**, 304.
3. Y. Wang, J. Di, L. Wang, X. Li, N. Wang, B. Wang, Y. Tian, L. Jiang and J. Yu, *Nat. Commun.*, 2017, **8**, 575.
4. *Switchable and Responsive Surfaces and Materials for Biomedical Applications*, Elsevier, Cambridge, UK, 2015.
5. H. Omichi, A. Katakai, T. Sugo and J. Okamoto, *Sep. Sci. Technol.*, 1985, **20**, 163-178.
6. N. Seko, A. Katakai, M. Tamada, T. Sugo and F. Yoshii, *Sep. Sci. Technol.*, 2004, **39**, 3753-3767.
7. D. Roy, M. Semsarilar, J. T. Guthrie and S. Perrier, *Chemical Society Reviews*, 2009, **38**, 2046-2064.
8. D. Braun, H. Cherdron, M. Rehahn and B. Voit, *Polymer Synthesis: Theory and Practice*, Springer, 5 edn., 2013.
9. C. W. Abney, R. T. Mayes, T. Saito and S. Dai, *Chem. Rev.*, 2017, **117**, 13935-14013.
10. B. F. Parker, Z. Zhang, L. Rao and J. Arnold, *Dalton. Trans.*, 2018, DOI: 10.1039/C7DT04058J.
11. M. Kanno, *J Nucl Sci Technol*, 1984, **21**, 1-9.
12. A. D. Kelmers, *Sep. Sci. Technol.*, 1981, **16**, 1019-1035.
13. J. Kim, C. Tsouris, R. T. Mayes, Y. Oyola, T. Saito, C. J. Janke, S. Dai, E. Schneider and D. Sachde, *Sep. Sci. Technol.*, 2013, **48**, 367-387.
14. S. Brown, Y. Yue, L.-J. Kuo, N. Mehio, M. Li, G. Gill, C. Tsouris, R. T. Mayes, T. Saito and S. Dai, *Ind. Eng. Chem. Res.*, 2016, **55**, 4139-4148.
15. S. Das, Y. Oyola, R. T. Mayes, C. J. Janke, L. J. Kuo, G. Gill, J. R. Wood and S. Dai, *Ind. Eng. Chem. Res.*, 2016, **55**, 4103-4109.
16. S. Das, Y. Oyola, R. T. Mayes, C. J. Janke, L. J. Kuo, G. Gill, J. R. Wood and S. Dai, *Ind. Eng. Chem. Res.*, 2016, **55**, 4110-4117.
17. T. Saito, S. Brown, S. Chatterjee, J. Kim, C. Tsouris, R. T. Mayes, L.-J. Kuo, G. Gill, Y. Oyola, C. J. Janke and S. Dai, *J. Mater. Chem. A*, 2014, **2**, 14674-14681.
18. F. Endrizzi, A. Melchior, M. Tolazzi and L. Rao, *Dalton. Trans.*, 2015, **44**, 13835-13844.
19. A. S. Ivanov and V. S. Bryantsev, *Dalton. Trans.*, 2016, **45**, 10744-10751.
20. N. Mehio, M. A. Lashely, J. W. Nugent, L. Tucker, B. Correia, C.-L. Do-Thanh, S. Dai, R. D. Hancock and V. S. Bryantsev, *J. Phys. Chem. B*, 2015, **119**, 3567-3576.
21. S. Vukovic, B. P. Hay and V. S. Bryantsev, *Inorg. Chem.*, 2015, **54**, 3995-4001.
22. S. Vukovic, L. A. Watson, S. O. Kang, R. Custelcean and B. P. Hay, *Inorg. Chem.*, 2012, **51**, 3855-3859.
23. E. G. Witte, K. S. Schwochau, G. Henkel and B. Krebs, *Inorg. Chim. Acta*, 1984, **94**, 323-331.
24. G. Tian, S. Teat and L. Rao, *Dalton. Trans.*, 2013, **42**, 5690-5696.
25. C.-Z. Wang, J.-H. Lan, Q.-Y. Wu, Q. Luo, Y.-L. Zhao, X.-K. Wang, Z.-F. Chai and W.-Q. Shi, *Inorg. Chem.*, 2014, **53**, 9466-9476.

26. C. W. Abney, R. T. Mayes, M. Piechowicz, Z. Lin, V. Bryantsev, G. M. Veith, S. Dai and W. Lin, *Energy Environ. Sci.*, 2016, **9**, 448-453.
27. C. W. Abney, S. Das, R. T. Mayes, L.-J. Kuo, J. Wood, G. Gill, M. Piechowicz, Z. Lin, W. Lin and S. Dai, *Phys. Chem. Chem. Phys.*, 2016, **18**, 23462-23468.
28. H. Omichi, A. Katakai, T. Sugo, J. Okamoto, S. Katoh, K. Sakane, K. Sugasaka and T. Itagaki, *Sep. Sci. Technol.*, 1987, **22**, 1313-1325.
29. Y. Oyola, C. J. Janke and S. Dai, *Ind. Eng. Chem. Res.*, 2016, **55**, 4149-4160.
30. H. Omichi, A. Katakai, T. Sugo and J. Okamoto, *Sep. Sci. Technol.*, 1986, **21**, 299-313.
31. T. Kawai, K. Saito, K. Sugita, A. Katakai, N. Seko, T. Sugo, J.-i. Kanno and T. Kawakami, *Ind. Eng. Chem. Res.*, 2000, **39**, 2910-2915.
32. T. Kawai, K. Saito, K. Sugita, T. Kawakami, J.-i. Kanno, A. Katakai, N. Seko and T. Sugo, *Radiat. Phys. Chem.*, 2000, **59**, 405-411.
33. J. Kim, Y. Oyola, C. Tsouris, C. R. Hexel, R. T. Mayes, C. J. Janke and S. Dai, *Ind. Eng. Chem. Res.*, 2013, **52**, 9433-9440.
34. C. Ibergay, P. Malfreyt and D. J. Tildesley, *J Phys Chem B*, 2010, **114**, 7274-7285.
35. B. Brettmann, P. Pincus and M. Tirrell, *Macromolecules*, 2017, **50**, 1225-1235.
36. J. Yu, J. Mao, G. Yuan, S. Satija, Z. Jiang, W. Chen and M. Tirrell, *Macromolecules*, 2016, **49**, 5609-5617.
37. C.-C. Cheng, F.-C. Chang, H.-C. Yen, D.-J. Lee, C.-W. Chiu and Z. Xin, *ACS Macro Letters*, 2015, **4**, 1184-1188.
38. C. B. Tang, T. Kowalewski and K. Matyjaszewski, *Macromolecules*, 2003, **36**, 8587-8589.
39. M. Kopec, P. Krysz, R. Yuan and K. Matyjaszewski, *Macromolecules*, 2016, **49**, 5877-5883.
40. A. Porcheddu and G. Giacomelli, in *The Chemistry of Hydroxylamines, Oximes and Hydroxamic Acids*, John Wiley & Sons, Ltd, 2008, DOI: 10.1002/9780470741962.ch6, pp. 163-231.
41. F. Eloy and R. Lenaers, *Chem. Rev.*, 1962, **62**, 155-183.
42. M. A. Silver, W. L. Dorfner, S. K. Cary, J. N. Cross, J. Lin, E. J. Schelter and T. E. Albrecht-Schmitt, *Inorg. Chem.*, 2015, **54**, 5280-5284.
43. P. S. Barber, S. P. Kelley and R. D. Rogers, *RSC Adv.*, 2012, **2**, 8526-8530.
44. M. A. Lashley, N. Mehio, J. W. Nugent, E. Holguin, C.-L. Do-Thanh, V. S. Bryantsev, S. Dai and R. D. Hancock, *Polyhedron*, 2016, **109**, 81-91.
45. B. Ravel and M. Newville, *J. Synchrotron Radiat.*, 2005, **12**, 537-541.
46. J. J. Rehr and R. C. Albers, *Rev. Mod. Phys.*, 2000, **72**, 621-654.
47. J. K. Zhao, C. Y. Gao and D. Liu, *J. Appl. Crystallogr.*, 2010, **43**, 1068-1077.
48. O. Arnold, et al., *Nucl. Instrum. Methods Phys. Res., Sect. A*, 2014, **764**, 156-166.
49. N. F. A. van der Vegt and D. Nayar, *J. Phys. Chem. B*, 2017, DOI: 10.1021/acs.jpcc.7b06453.
50. Y. Yue, R. T. Mayes, J. Kim, P. F. Fulvio, X.-G. Sun, C. Tsouris, J. Chen, S. Brown and S. Dai, *Angew. Chem. Int. Ed.*, 2013, **52**, 13458-13462.
51. Y. Yue, C. Zhang, Q. Tang, R. T. Mayes, W.-P. Liao, C. Liao, C. Tsouris, J. J. Stankovich, J. Chen, D. K. Hensley, C. W. Abney, D.-e. Jiang, S. Brown and S. Dai, *Ind. Eng. Chem. Res.*, 2015, **55**, 4125-4129.
52. D. R. M. Williams, *J. Phys. II France*, 1993, **3**, 1313-1318.
53. W. C. Hamilton, *Acta Crystallographica*, 1965, **18**, 502-510.
54. L. Downward, C. H. Booth, W. W. Lukens and F. Bridges, *AIP Conf. Proc.*, 2007, **882**, 129-131.
55. S. Calvin, *XAFS for Everyone*, CRC Press, Boca Raton, FL, 2013.
56. L. Zhang, J. Su, S. Yang, X. Guo, Y. Jia, N. Chen, J. Zhou, S. Zhang, S. Wang, J. Li, J. Li, G. Wu and J.-Q. Wang, *Ind. Eng. Chem. Res.*, 2016, **55**, 4224-4230.
57. S. D. Kelly, K. M. Kemner, J. B. Fein, D. A. Fowle, M. I. Boyanov, B. A. Bunker and N. Yee, *Geochim. Cosmochim. Acta*, 2002, **66**, 3855-3871.
58. A. I. Frenkel, M. Vairavamurthy and M. Newville, *J Synchrotron Radiat*, 2001, **8**, 669-671.
59. B. P. Grady, E. M. O'Connell, C. Z. Yang and S. L. Cooper, *J. Polym. Sci. Part B Polym. Phys.*, 1994, **32**, 2357-2366.
60. J. A. Hammons, J. Ilavsky and F. Zhang, in *Electrochemistry in Ionic Liquids: Volume 1: Fundamentals*, ed. A. A. J. Torriero, Springer International Publishing, Cham, 2015, DOI: 10.1007/978-3-319-13485-7_6.
61. B. Qiao, G. Ferru, M. Olvera de la Cruz and R. J. Ellis, *ACS Cent. Sci.*, 2015, **1**, 493-503.
62. R. J. Ellis, Y. Meridiano, J. Muller, L. Berthon, P. Guilbaud, N. Zorz, M. R. Antonio, T. Demars and T. Zemb, *Chem. Eur. J.*, 2014, **20**, 12796-12807.
63. R. J. Ellis, T. L. Anderson, M. R. Antonio, A. Braatz and M. Nilsson, *J. Phys. Chem. B*, 2013, **117**, 5916-5924.
64. S. P. Kelley, P. S. Barber, P. H. K. Mullins and R. D. Rogers, *Chem. Commun.*, 2014, **50**, 12504-12507.
65. S. Vukovic and B. P. Hay, *Inorg. Chem.*, 2013, **52**, 7805-7810.